Analysis of Parabolic Leaf Spring Failure

Perttu Kainulainen

Thesis

Bachelor's degree

Savonia
University of Applied Sciences

SAVONIA-AMMATTIKORKEAKOULU **OPINNÄYTETYÖ**

Tiivistelmä

Koulutusala Tekniikan ja liikenteen ala		
Koulutusohjelma Kone- ja tuotantotekniikan koulutusohjelma		
Työn tekijä(t) Perttu Kainulainen		
Työn nimi Lehtijousen vaurioanalyysi		
Päiväys 29.4.2011	Sivumäärä/Liitteet	45
Ohjaaja(t) Lehtori Pertti Kupiainen, R&D Manager Jyrki Kulmala, R&D Engineer Pekka Holopainen		
Toimeksiantaja/Yhteistyökumppani(t) Normet Group		

Tiivistelmä

Työn tarkoituksena oli tehdä parabeelisen lehtijousen vaurioanalyysi. Lehtijousi on käytössä kaivosajoneuvossa, joka on tarkoitettu henkilöstön ja varusteiden kuljetukseen kaivoksissa. Analyysissä tutkittiin jouseen tehdyn parannuksen vaikutusta ja ilmiöitä, jotka aiheuttivat vaurion.

Teoreettisessa vaiheessa ongelmaa lähestyttiin dynamiikan simulointia ja elementtimenetelmää hyväksi käyttäen. Dynamiikan si-mulointi mahdollisti jousen voimavuon määrityksen. Voimia käytettiin tämän jälkeen elementti-menetelmä laskennassa. Kokeellisessa vaiheessa jousen jännitykset tarkastelupisteessä määri-teltiin venymäliuskamittausten avulla. Mittauksista saatuja kuormitustietoja käytettiin jousen kestoiän laskentaan.

Saaduista laskenta- ja mittaustuloksista pystyttiin selvittämään jousen todennäköinen katkeamissyy. Tuloksilla pystyttiin perustelemaan jousen konstruktion muutoksen tarve. Lopputuloksena projektista saatiin ajoneuvoon uuden jousimallin prototyypin.

Avainsanat
parabeelinen lehtijousi, FEM, FEA, MBS, dynamiikan simulointi, väsyminen, venymäliuska

Julkinen

SAVONIA UNIVERSITY OF APPLIED SCIENCES **THESIS**

Abstract

Field of Study Technology, Communication and Transport			
Degree Programme Degree Programme in Mechanical Engineering			
Author(s) Perttu Kainulainen			
Title of Thesis Analysis of Parabolic Leaf Spring Failure			
Date	29 April 2011	Pages/Appendices	45
Supervisor(s) Mr.Pertti Kupiainen, M.Sc, Mr.Jyrki Kulmala, R&D Manager, Mr.Pekka Holopainen, R&D Engineer			
Project/Partners Normet Group			

Abstract

The purpose of this final project was to make an the fracture analysis for a parabolic leaf spring. The leaf spring type is used in a mining machine. The machine is designed for personnel and equipment transportation in a mine environment. The objectives were to gather information about effects of the improvement in the spring' structure and study phenomena which eventually lead to the fracture of the spring.

The project was divided into theoretical and experimental sections. The theoretical section included dynamic simulation with the multibody system approach and the finite element analysis. The multibody system was used to determine of the force flux of the spring. Values of the force flux were used as input forces in the finite element analysis. The experimental section consisted of strain gage measurements. Strain gage measurements were used to define stress levels in the examination point. The fatigue life time of the spring was calculated by using the loading history from measurements.

The cause of the spring fracture was defined from results, produced by calculations and measurements. The results were also used as a criterion for the change of the spring type. As a final result, the project produced prototypes for new springs.

Keywords
parabolic leaf spring, FEM, FEA, MBS, dynamic simulation, fatigue, strain gage

Public

FOREWORDS

I would like to express my gratitude to Pertti Kupiainen, M.Sc, Jyrki Kulmala, R&D Manager and Pekka Holopainen, R&D Engineer for all the guidance, help and advises during the project.

In addition, I want to thank Mr. Mikko Huusko, B.Sc from Savonia University of Applied Science for the assistance in the installation of strain gages. I am also grateful to all those persons at Normet who helped me during this project.

In Kuopio 29 April 2011

Perttu Kainulainen

TABLE OF CONTENTS

VARIABLES, UNITS AND ABBREVIATIONS

E	Young's modulus of elasticity, MPa
G	Shear modulus, MPa
ν	Poison's constant
F	Force, N
F_x	Normal force in x-axis, MPa
F_y	Normal force in y-axis, MPa
F_z	Normal force in z-axis, MPa
M	Moment, Nm
M_x	Moment over x-axis, Nm
m	Mass, kg
m_s	Sprung mass, kg
m_u	Unsprung mass, kg
ε	Strain, mm/mm
k	Gage factor
ε_m	Mass ratio
ω	Angular velocity, 1/s
σ	Stress, MPa
σ_{ekv}	Equivalent (von Mises) stress, MPa
σ_x	Principal stress x-axis, MPa
σ_y	Principal stress y-axis, MPa
σ_z	Principal stress z-axis, MPa
σ_p	Proportional limit, MPa
σ_e	Elastic limit, MPa
σ_w	Endurance limit, tension, MPa
σ_{bw}	Endurance limit, bending, MPa
τ_{wv}	Endurance limit, torsion, MPa
R_{eL}	Yield limit, Lower, MPa
R_{eH}	Yield limit, Higher, MPa
R_m	Ultimate stress, MPa
v	Transitional velocity, m/s
U_{oD}	Distortion energy
W	Bending resistance, mm^3
I_x	Second moment of area (in respect of neutral axis), mm^4
R	Resistance, Ω
ΔT	Duration of test, s
L	Fatigue life time, s

L_{bmp}	Fatigue life time, maximum principal stress with respect to bending, s
L_{bekv}	Fatigue life time, von Mises stress with respect to bending, s
L_{ε}	Fatigue life time, Stain-life, s
N_i	Life cycles in S-N curve
n_i	Load count in rainflow
K	Work hardening coefficient, MPa
$S_{f'}$	Fatigue strength coefficient, MPa
K'	Cyclic strength coefficient, MPa
N	Work hardening exponent,
b	Fatigue strength exponent
c	Fatigue ductility exponent
$E_{f'}$	Fatigue ductility coefficient
n'	Cyclic strain-hardening exponent
N_c	Cut-off, Reversals

RBO	Mining vehicle, designed for personnel and equipment transportation in a mine environment.
FEA	Finite Element Analysis
FEM	Finite Element Method
MBS	Multibody System
CAD	Computer Aided Design
JIS	Japanese Industrial Standards

1 INTRODUCTION

The purpose of this final year project is to analyse leaf spring failure. The client for this project is the R&D department of Normet Group. The spring is used in the RBO underground mining machine, manufactured by Normet Corporation. Chapter 2.2 introduces RBO.

The main objective is to gather information about the effect of the improvement on the spring structure. The secondary objective is to get information about the phenomena which have effect on the fracture of the spring. The assumption at the start of the project is that the spring takes quite a high twisting torque around longitudinal direction. The twisting torque is generated from inertial forces of the vehicle body mass. The situation at the beginning of this project is that the life time of a single spring is too low. The duration of one spring, according to customers' report, was from 100 hours to few months. The most common fracture point was located close to the spring eye in the fixed support side where the profile is thinnest. The broken spring is presented in Figure 1. The improved structure of the spring is shown in Figure 2.

Figure 1. Broken spring in the front axle. (Normet Group)

Figure 2. Spring with the clamp installed. (Normet Group, Marketing databank)

The analysis will be carried out by using different kinds of approach methods. The process flow of the analysis is presented in Figure 3. The project was divided into theoretical and experimental sections. The theoretical phase consists of the multi-body system (MBS) and the finite element (FE) approach. The experimental phase consists of series of strain gage measurements to analyses stress levels and to predict the life cycle of the spring. The basic idea is to collect data from different outputs to verify and compare the results.

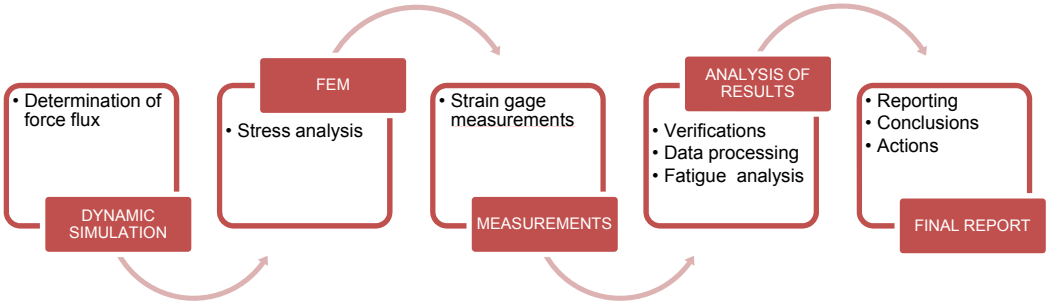

Figure 3. Process of the analysis.

2 BACKGROUND

2.1 Normet Group

Normet provides solutions for underground mining and tunnelling. Projects are mostly done according to the customers' needs and final products are designed to execute needs of the mass customization. Their main products are in the field of concrete spraying, charging, scaling, lifting, installation and underground logistics processes. Normet also provides Life Time Care (LTC) services which includes spare parts, maintenance, repairing, training and tunnelling process expertise. The organisation structure is presented in Figure 4. Main facilities are located in Iisalmi, Finland. The group has several offices around the globe. The global organization includes sales and distribution offices in every major market area. The company has also manufacturing, customization and repair workshops in Chile, Australia and North America. Chile is manufacturing Semmco's products which is a subsidiary. Farmi Forest is also part of the Normet Group as a subsidiary. Farmi Forest is specialised in the development and manufacturing of forest machines which can be installed in tractors. The product family consists of winches, wood chippers, cranes and firewood processors. (Normet Group, Company presentation),(Normet Group, Press release)

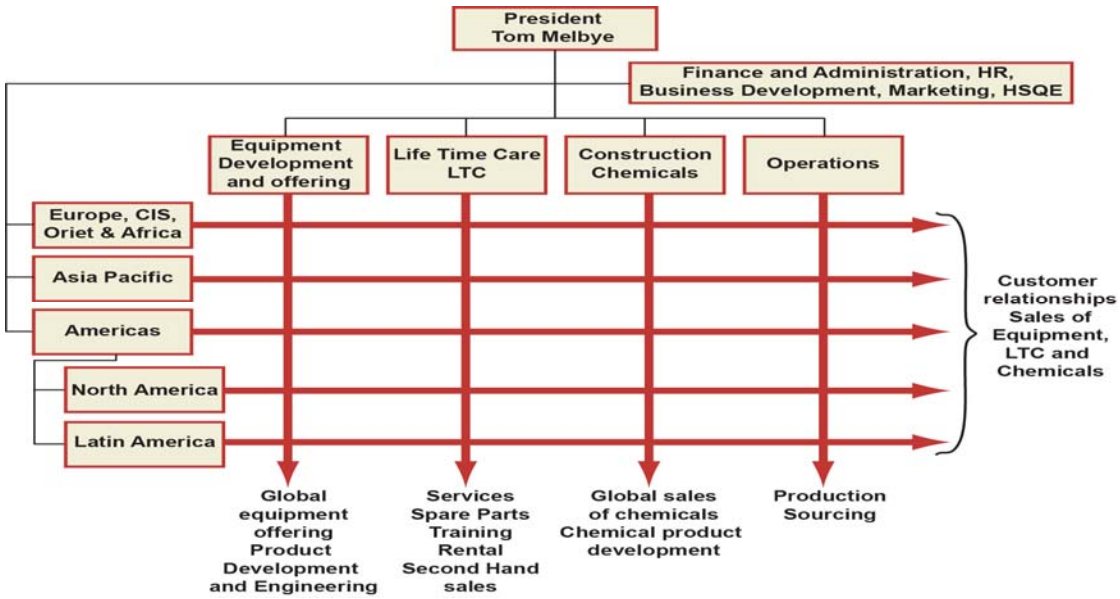

Figure 4. Normet's global structure. (Normet Group, Company presentation)

The Normet Group is one of the leading manufacturers and service providers in its own marketing segment. Over 90% of the production goes to export. The distribution of net sales by product groups is presented in Figure 5. The company's turnover was 117 million euro in year 2010 and it employs over 600 persons. (Normet Group, Company presentation)

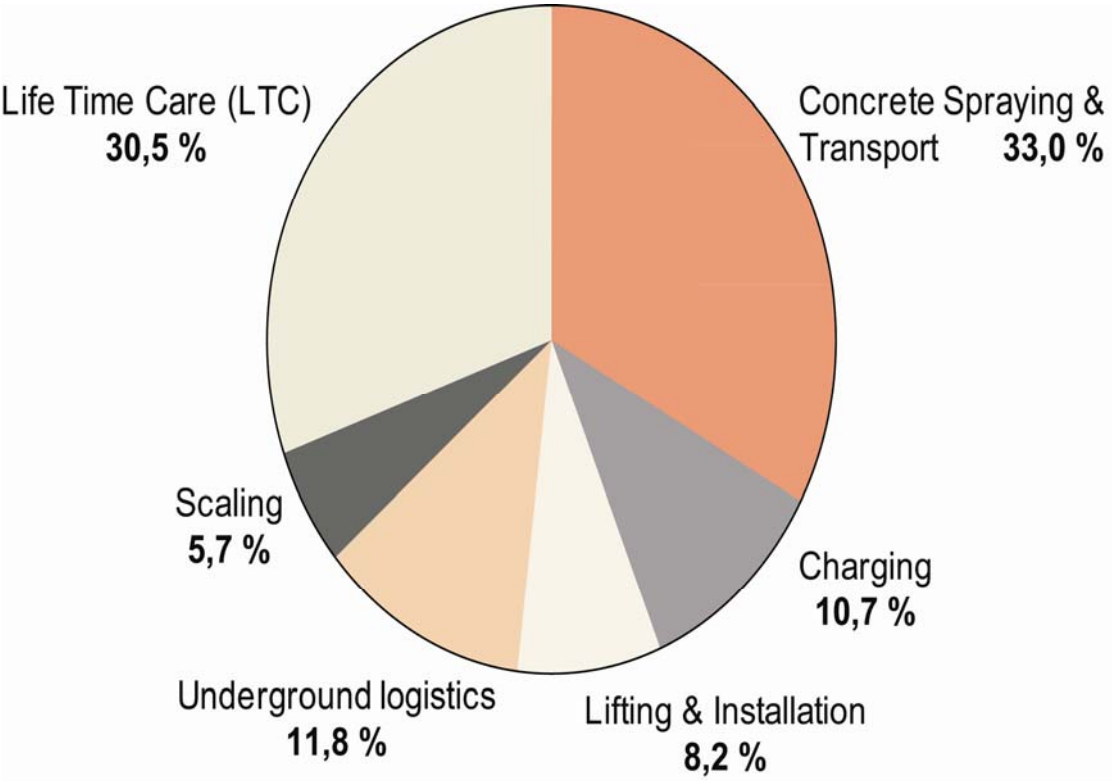

Figure 5. Net sales distribution by product groups in 2010. (Normet company presentation)

2.2 RBO

The RBO is designed for underground transportation for personnel and equipment. Personnel and equipment are usually transported in the mine by using vehicles not designed for underground use. Ordinary machines like pick-up cars and tractors do not provide safe solution to underground conditions. These vehicles are also under constant repairs and cause stoppage time. The idea is to provide save and robust solution which has the same characteristics than ordinary cars. RBO is presented in Figure 6. (Kulmala, 2005)

The RBO is powered by a 95 kW diesel engine. It is capable of carrying five persons and a cargo if 1000 kg. The power transmission has been engineered by using a hydrostatic transmission. The transmission consists of the flywheel driven pump and the axial-piston motor. The hydrostatic transmission gives a wide range of speed and torque. Operating conditions are irregular and it sets special requirements for suspension. In this vehicle the suspension has been engineered by using parabolic leaf springs. RBO's axle structure has been designed with solid axles which are mounted to a frame by using leaf springs. This design is called the Hotchkiss drive. The construction and mechanics of the Hotchkiss drive are explained in Chapter 3.1. (Kulmala, 2005)

Figure 6. RBO

3 THEORY

3.1 Suspension Mechanics

Suspension can be considered as a link between the wheels and the body. It absorbs quick loadings and collects the elastic energy. Design fundamentals are based on the strength and comfort. The strength characteristics are usually determined according to the suspension type and loading. The comfort design fundamentals originate from the fluctuation and vibration point of view. The basic idea for the design is to generate the wanted elasticity and maintain the driving comfort. The leaf spring is one of the oldest suspension types. Nowadays it is widely used in heavy duty vehicles and work machines. The advantages of the leaf spring are based on its simple construction, low costs and easy maintenance. The design also provides the solution for the axle support. RBO's suspension uses parabolic leaf springs. The difference between the normal leaf spring and the parabolic leaf spring is the total number of leafs. A parabolic leaf does not need of huge amount of leafs because the stress is distributed equally due to its parabolic shape. Examples of the parabolic and the standard leaf spring are presented in Figure 7. (Zahavi & Barlam 2001, 265)

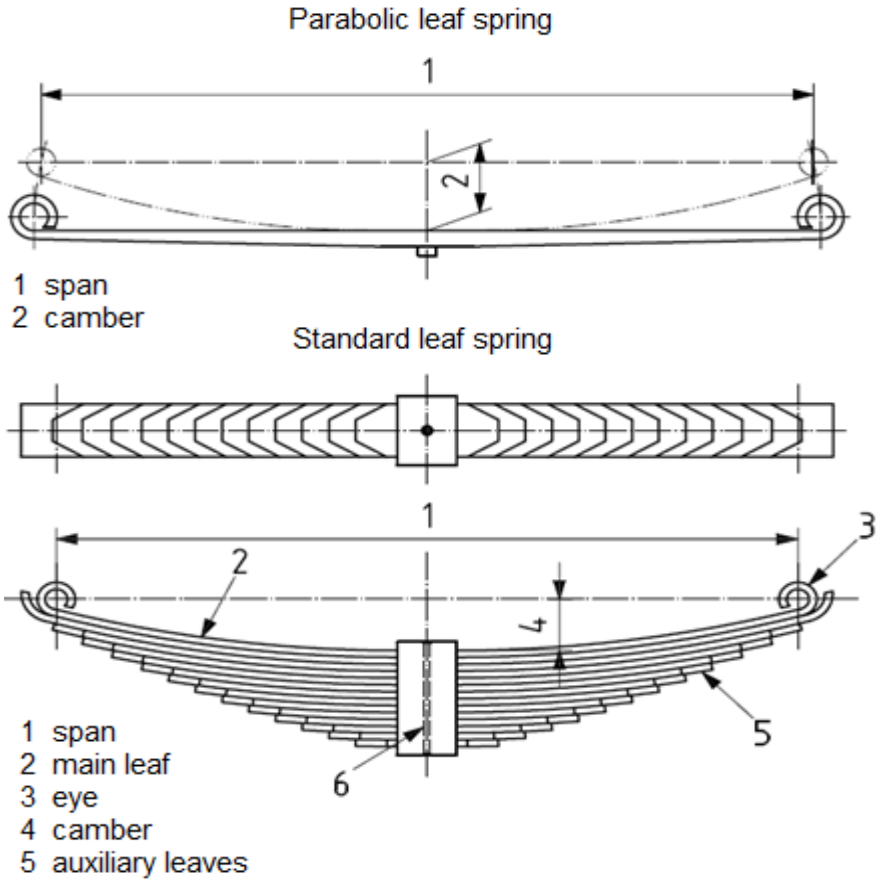

Figure 7. Standard and parabolic leaf spring. (ISO 26909:2009)

The leaf spring has a bending stress which must be equally distributed along the structure. In mathematical point of view, the leaf spring can be considered as a cantilever beam. The bending stress in the arbitrary distance *x* can be expressed with the equation

$$\delta_{t_x} = \frac{M_t}{W} = \text{constant} \quad (1)$$

where M_t is bending moment and W is bending resistance. This equation qualifies for a spring which has regular cross-section area. Bending stress σ_t for the parabolic leaf spring can be expressed with the equation

$$\delta_t = \frac{M_x h_x}{I_x 2} \quad (2)$$

where M_x is the bending moment, h_x is the thickness of the leaf and I_x is the second moment of a area. I_x and h_x are usually expressed as functions in the parabolic leaf. $I_x=f(x)$ and $h_x=f(x)$. (Laine 1981, 121)

The RBO suspension has been engineered with the Hotchkiss drive, introduced in Figure 8. In the Hotchkiss's drive, the solid axle and wheels are mounted to a frame with two leaf springs.

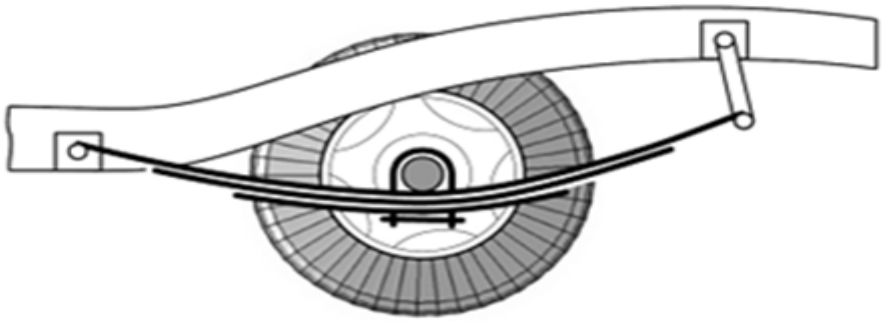

Figure 8. The Hotchkiss drive. (Jazar 2008 ,456)

The Hotchkiss drive is the simplest solution for suspension and linkage between the frame and axle. The solution has problematic dynamics which are due to low mass

ratio. The mass ratio means relation between the supported and unsupported mass and it can be expressed with the equation

$$\varepsilon_m = \frac{m_u}{m_s} \tag{3}$$

where m_s is the mass of bodies, which are supported by a spring, like the vehicle's body. m_u is the mass of those bodies that are mounted to a spring but not supported, like axle and tyres. In this construction springs are acting as a locating member. Demanded property of the spring is to flex under loading to the one direction. In Hotchkiss's drive the leaf spring goes under lateral and longitudinal loading. This usually leads to a situation where the spring is bended to a so called S curve, when braking and accelerating. Braking and accelerating situations are demonstrated in Figure 9. Inertial forces of the frame and body are also creating longitudinal twisting torque to the spring. (Jazar 2008, 456-457)

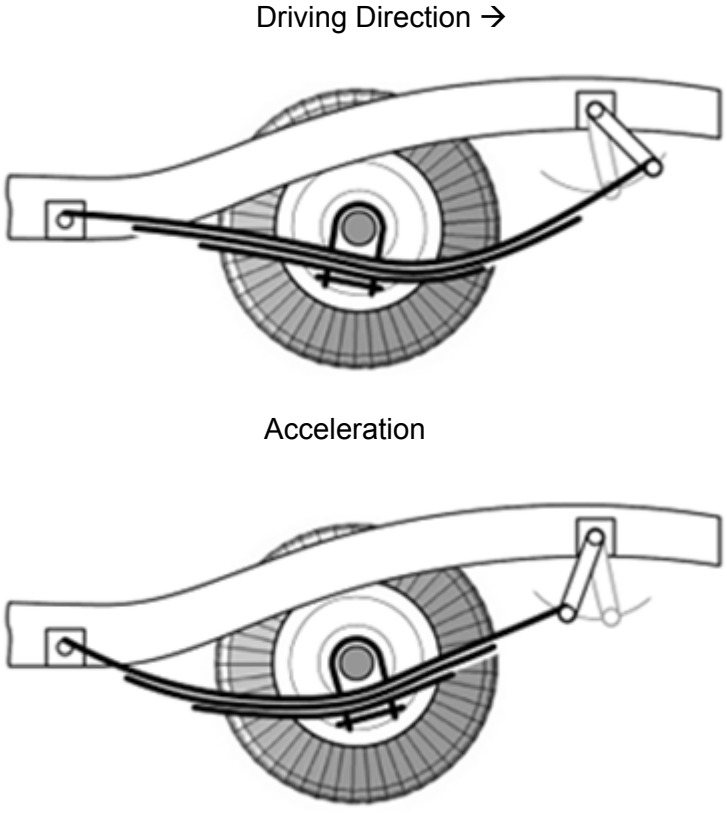

Figure 9. The S curve in acceleration and braking. (Jazar 2008, 457)

3.2 Dynamic Simulation

One of the tools used in this project was the dynamic simulation which was based on the multibody system analysis. Dynamic simulations have been used for decades by dividing one complex to subsystems. Older procedures were inaccurate because the behaviour of the one subsystem has an effect on other systems. The development of numerical modelling methods has made it possible to analyse systems as a one complex. This has lead to the development of multibody system (MBS). The modelling of the complex system has been carried out by using so called Lagrange's method. Lagrange's method makes it possible to model the mechanism by using generalised coordinates. (Rouvinen 2003, 7-8)

The multibody system approach has been used for several years to analyse machines and mechanics. The MBS is widely used as a R&D and training simulator. The system gives possibilities to simulate a machine or mechanism in real-time in the concept design phase. The simulation is able to predict and confirm the behaviour of the machine before the actual prototype is created. The software allows the connection of real control devices to the simulation. This has made it possible to implement a relatively realistic training in the virtual environment. (Korkealaakso 2009, 13-15)

The basic dynamic model consists of determinations of body types, constrain equations and forces. Known forms of bodies are rigid, dummy and flexible bodies. Rigid and dummy bodies are only using terms of inertia and mass properties. Flexible bodies are defined by superposing the natural frequency shapes. Constrain equations are used to connect bodies and express the movement mechanism with respect to joint behaviour. An example of the cylindrical constrain is presented in Figure 10. Position vectors of bodies are expressed with respect to the global coordinate system. (Korkealaakso 2009, 13-15)

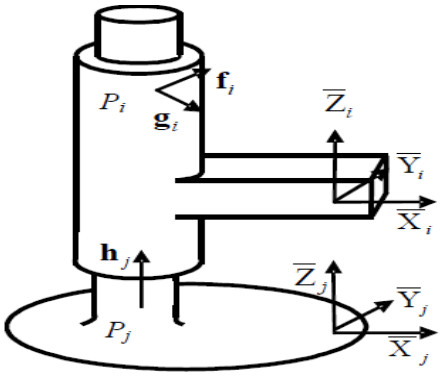

Figure 10. Cylindrical constrain. (MeVEA OY)

3.3 Dynamic Model of RBO

Normet is using software which has been developed by the MeVEA Oy. The simulation model of the RBO was created to the program by the MeVEA Oy. The model was defined by using rigid, dummy and flexible bodies. Rigid and dummy bodies where modelled by using parameters such as mass, centre of mass and inertia properties. Springs were modelled as flexible bodies. Simplifications of the model where that, joint clearances and the friction are not modelled, all bodies, except springs, are absolutely rigid, steering hydraulics are modelled as a spring-damper force, a hydraulic pressure is distributed evenly in the hydraulic volume and the power transmission does not include coefficients. Topology of the dynamic model is shown in Figure 11.

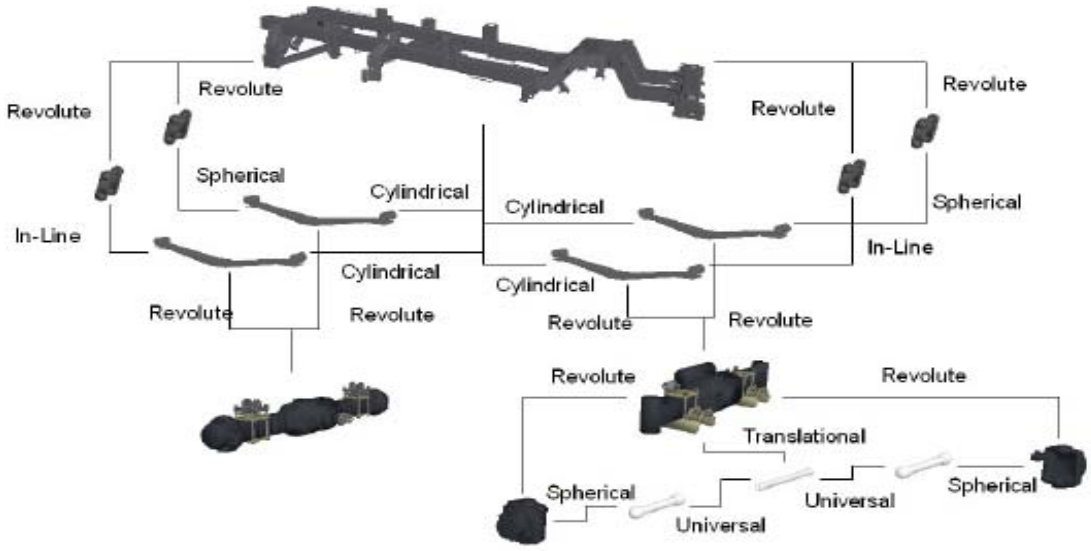

Figure 11. Structure of the dynamic model.

The simulation allowed examination of forces and moments affecting to bodies and constrains. In this case, the computing constrain was between the spring and axle. The simulation environment was created to correspond to the realistic mine environment where vehicle is under constant curve drive. Idea of curve drive was to generate affect of inertial forces. Impact analysis was created to the outdoor environment which enabled desired control directions to the impact. Simulation environments are presented in Figures 13 and 14.

Figure 13. Virtual outdoor environment of the dynamic simulation.

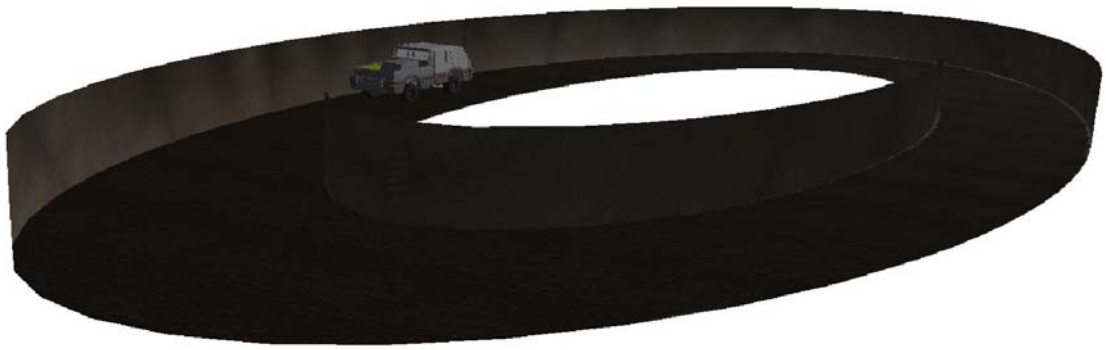

Figure 14. Virtual mine environment of dynamic simulation.

3.4 Finite Element Method

The finite element method (FEM) or the finite element analysis (FEA) are an analysis methods to solve complex problems that cannot be described in the traditional engineering science. Fundamentals of the FEA are to divide a complex problem to several smaller problems and then use mathematics as a tool to bind solutions. The combined solution will give approximate determination for the complex solution. The development of the FEA was originated in 1960 by civil and aeroplane engineering industries. When the civil aviation started to grow up the need for safe structures increased. This led to the research of numerical modelling methods using the computers. (Mac Donald 2007, 47)

The typical flowchart of the FEA is shown in Figure 15. This process can be applied to any kind of analyses which are performed by using the FEA. The process starts of the determination of the physical problem. The FEA can be considered as a powerful tool to solve issues related to the engineering science, but it requires understanding of the physical problem. After the determination of the physical problem the mathematical model can be created. This means definitions of mathematical formulations and the problems physical outlines. The discretion of the model is usually defined in FEA programs by the automatic tool. Programs are capable to create elements without the user definitions. Even though, the automatic meshing and elements are implemented to programs, they are not able to predict where the finer mesh is needed. Refining of the mesh is usually done by using the information from the determination of the physical problem. Computational methods and strategies are mostly based on the user experience. Definitions are required when selecting solution methods, time steps or load steps for non-linear analysis. The solution of the model is processed when all definitions are done. The product from the solution is a result or an error. The post-processing offers information for rejecting or acceptance of the analysis. Processing of the data is usually done within the limits of knowledge of the physical problem. For example, common procedures in practical analyses are comparing the stress levels to material properties or inspect allowed displacements. Verifications can be done by using the previous information or experience. The data can be validated also via measurements if possible. (Mac Donald 2007, 47-50)

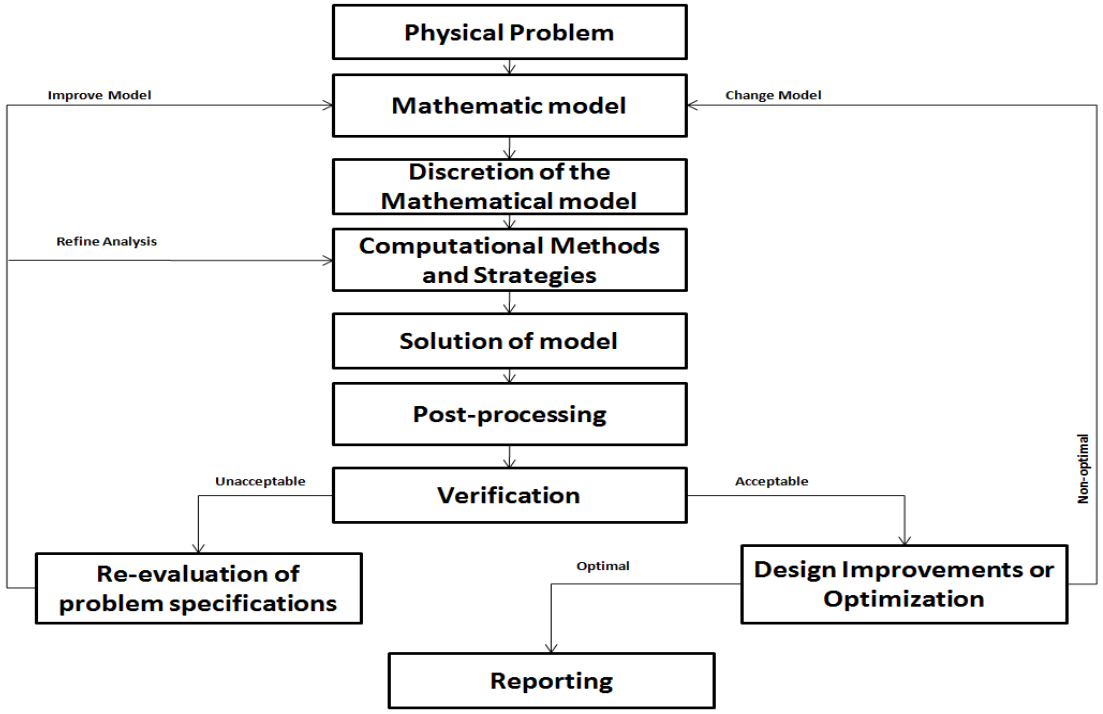

Figure 15. Process flowchart of typical FE-analysis. (Mac Donald 2007, 48)

3.5 FE Model of the Spring

The FE-model was created from the 3D model of the spring. Modelling was done by using the Autodesk Inventor 2010 CAD program. The analysis was done with the Ansys WorkBench 13.0. The assembly was determined with components which were essential for calculations. Interesting points for the analysis were the thinnest cross section areas in the spring profile. The 3D model is presented in Figure 16. Simplifications of the model were that elasticity of flexible bushings (3. in Figure 16) and rubber mount (6. in Figure 16) are not taken into account in the FE model. The contact friction between the rubber mount and the main spring is not modelled.

Boundary conditions are modelled into the spring's eyes by using the cylindrical and remote displacement supports. Supports and the global coordinate system are introduced in Figure 17. The cylindrical support in the point A allows rotation over the z-axis with respect to the global coordinate system. The remote displacement allows rotation over the z-axis and displacement along the x-axis in the global coordinate system.

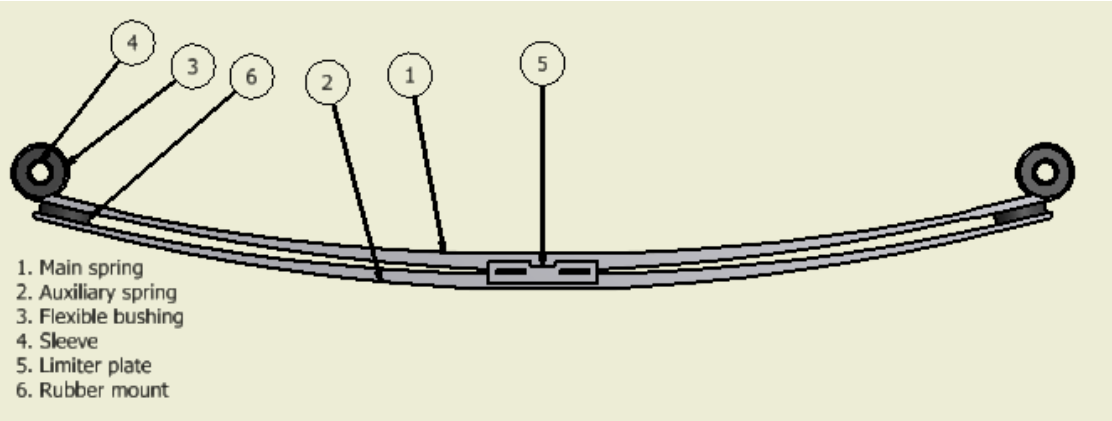

Figure 16. 3D-model of the spring.

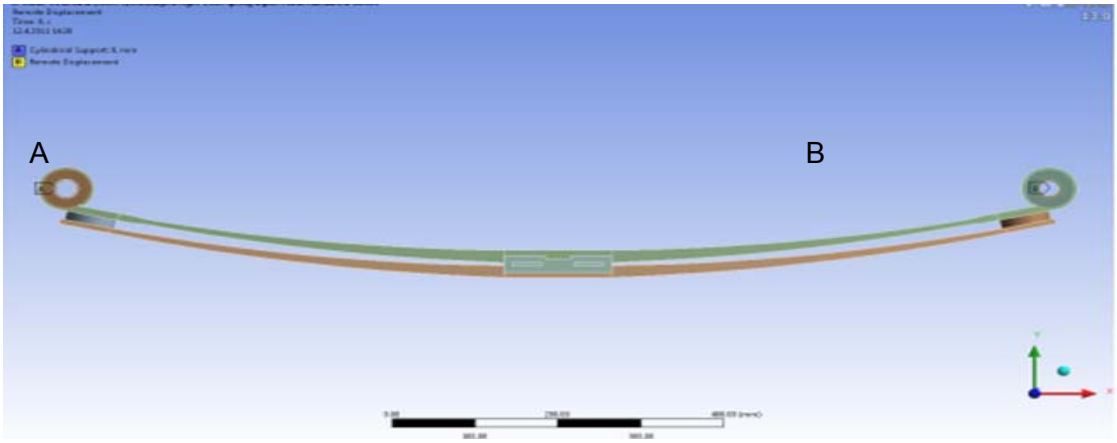

Figure 17. Supports of the spring.

The mesh was generated by using the Ansys workspace automatic tool. The tool generated automatic elements to solid bodies. The mesh was refined in examination and contact areas. Refining was also done for flanks of the spring. The meshed model of the spring is shown in Figure 18. Model contained 303256 nodes and 183984 elements.

Contacts of the model are bounded except for the contacts between rubber mounts and the main spring which are determined as frictionless connections. This type of connection describes the behaviour of the spring in an ideal state where the friction between leaves is not wanted. Contact settings of the frictionless connection are presented in Figure 19. The formulation type in the nonlinear contact was set to the augmented Lagrange. This is usually more appropriate for the nonlinear analysis. The interface treatment is set to be in 'Adjust to Touch' which ignores any initial penetration and creates the stress free state to contact surfaces. The time step control uses automatic bisection. This setting evaluates the contact behaviour at the end of each sub step. If penetration or drastic changes are detected the sub step is evaluated again with the time increment which is reduced by half.

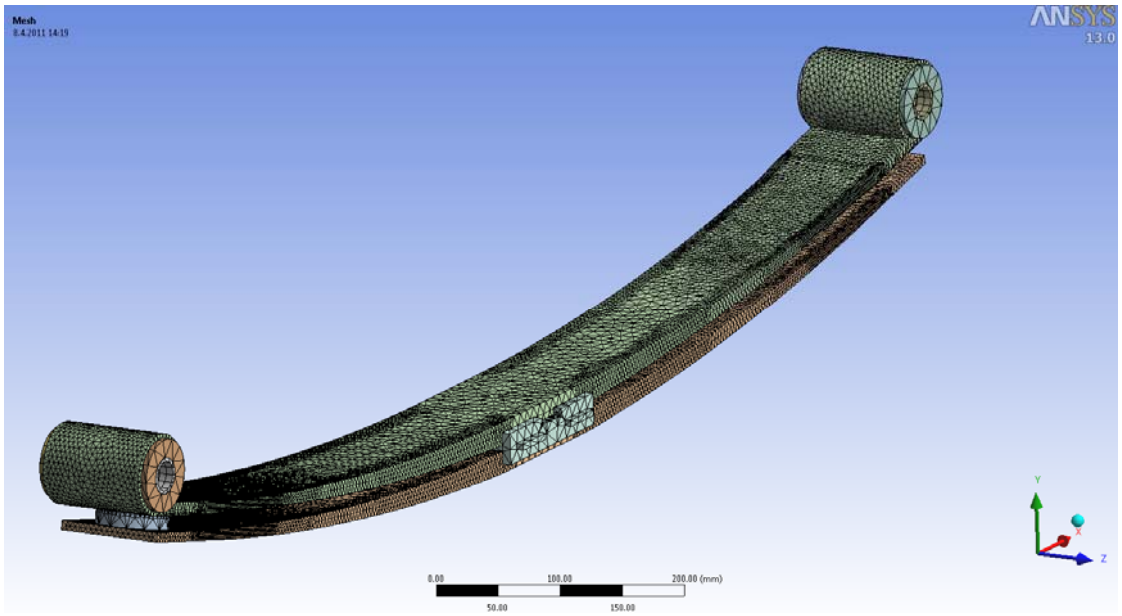

Figure 18. Meshed FE-model.

Scoping Method	Geometry Selection
Contact	1 Face
Target	1 Face
Contact Bodies	kumityyny:1
Target Bodies	rbo_päänorra etu:1
Definition	
Type	Frictionless
Scope Mode	Manual
Behavior	Symmetric
Suppressed	No
Advanced	
Formulation	Augmented Lagrange
Interface Treatment	Adjust to Touch
Normal Stiffness	Program Controlled
Update Stiffness	Never
Pinball Region	Program Controlled
Time Step Controls	Automatic Bisection

Figure 19. Contact setting of frictionless connection.

3.6 Strain Gages

Strain gages are instruments which measure strains in the material. The principle is based on assumption that the measured strain is transferred to a gage without any loss. It means that the gage and the object must be very close connected. Normally this is done by using adhesive attachment methods. In special cases the gage can be installed inside of the object. This is possible for example in the concrete where the gage is possible to install before the pouring. (Hoffmann 1989, 12)

The functionality of the metal strain gage is based on the relationship of the strain and resistance of electrical conductors. This phenomenon was first discovered by Wheatstone and Thomson. It points out that the electrical conductor resistance changes with the mechanical stress. When the microstructure of the material alters it causes deformation in the conductor and change in the resistivity of the conductor material. This can be expressed with the equation

$$\frac{dR}{R_0} = \varepsilon(1 + 2\upsilon) + \frac{dQ}{Q} \tag{4}$$

where R is a electrical resistance, ε a strain, υ a is Poisson's constant and Q is a resistivity. (Hoffman 1989, 13)

The Wheatstone bridge circuit enables accurate measurements of the electrical resistance. The bridge can be used to determine the absolute value of the resistance by compeering it with the known resistance or to solve relative change in the resistance. The determination of relative change can be exploited in strain gage measurements.

In this project, strain gages were connected to the quarter bridge with three wires. The circuit diagram of the bridge is presented in Figure 20.

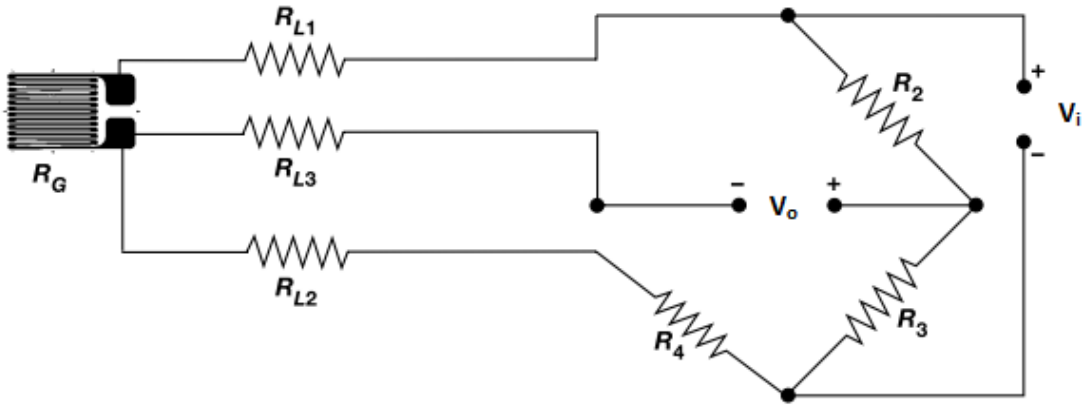

Figure 20. A three-wire connection in the quarter bridge. (Vishay MicroMeasurement. The three-wire quarter bridge circuit, Application note TT-612, 2005)

When the supply voltage is fed to the bridge in two points it will be processed as a ratio of the resistance. This means that the voltage is divided to both sides of the circuit. Resistances R_1, R_2 and R_3, R_4 are acting as a voltage divider. The connection assumes that the resistance of the voltage supply is small and the output voltage of the measuring instrument has a high internal resistance so it does not produce loading. When the bridge is not balanced it can be expressed in the equation

$$V_O = V_S\left(\frac{R_1}{R_1R_2} - \frac{R_4}{R_3R_4}\right) \tag{5}$$

where V_O is output voltage and V_i is input voltage. The equation shows difference of voltages from resistances. When the bridge is balanced the output voltage is zero. When leading the equation to the final state it has an expression

$$\frac{\Delta R}{R} = k\varepsilon \tag{6}$$

Where R is the resistance of the bridge, ΔR is the change of resistance, k is the gage factor and ε is the strain. (Hoffmann 1989, 126-129)

3.7 Hook's Law

One of the most important phenomena in material strength is the connection between stress and strain and ability to sustain loading without fracture. The stress and strain

connection is also known as a *σε*-curve or material equation. Material properties, like the yield strength and ultimate yield strength, are usually determined by the *σε*-curve as demonstrated in Figure 21. (Outinen, Salmi & Vulli 2007, 38)

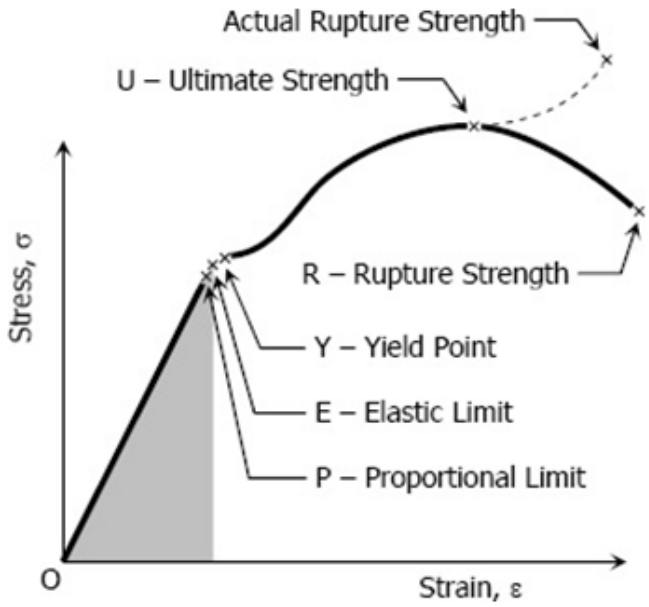

Figure 21. *σε*-curve of medium carbon steel. (http://www.mathalino.com)

Usually dimensioning with respect to the material strength is done by using values determined by the *σε*-curve. The curve describes points which are essential for the material deformation. Figure 21 indicates that the curve has a linear section from origin to the proportional limit σ_p. This was noticed by Sir Rober Hook in the late 1600-century. Hook stated that the stress-strain relationship is directly proportional in the linear part of the curve. This can be expressed with the equation

$$\delta = E\varepsilon \tag{7}$$

where E is the modulus of elasticity, σ is the stress and ε is the strain. In the machine design, the stress should not exceed the proportional limit. However, the accurate determination of the proportional limit is difficult and the design stress is usually determined by using the lower yield limit R_{eL}. Dimensioning also includes the safe factor which can be determined with the case sensitive point of view. The elastic limit σ_e is the point where the plastic deformation occurs and the material does not return in its original shape. The yield point describes a point where the material starts elongation without the dramatic increasing of loading. The rupture strength is a point where the material failure occurs. (Outinen 2007, 34-38)

3.8 Fatigue in Machine Design

Fatigue analyses are done to determine the fatigue strength of the structure. Analyses can predict the life cycles of elements which are under the variable amplitude loading. Most of the structural failures in machines are caused by the fatigue phenomena. First experimental analyses where done by August Wöhler. Wöhler stated that the loading cycle is determinant instead of the time taken to a fatigue experiment. Wöhler also stated that iron metals will last infinite loading cycles if the stress does not exceed the certain limit. The fatigue analysis can be considered as one of the most important criteria in designing machine components under the variable amplitude loading.

Static fractures can be overviewed from the control point. This means that the yield condition can be expressed by using the principal stress. The fatigue fracture has more complex determination. It is liable to material properties, stress state of control point and surrounding stress state field. The fatigue also includes several variables which cannot be specified easily. The theoretical processing of the fatigue fracture has not been able to determine precisely although there are several standards and calculation models which are describing the fatigue behaviour. (Outinen 2007, 367)

In this project the fatigue analysis was done by using the strength hypotheses and the rainflow method. The fatigue life predictions were also done by using the strain life based approach. The von Mises hypothesis describes the behaviour of viscous steel under the multiaxis stress state. The hypothesis points out that the fracture of material will occur at the point where the constant energy of distortion achieves the critical value for the material and the fracture type. When the elastic material is under loading it stores elastic energy. The portion of this energy goes to the deformation of volume. The rest of the energy is concentrated to the distortion of the shape. The distortion energy in the certain point can be expressed with the equation

$$U_{oD} = \frac{1}{12G}[(\delta_x - \delta_y)^2 + (\delta_y - \delta_z)^2 + (\delta_z - \delta_x)^2] + \frac{1}{2G}(\tau_{xy} + \tau_{yz} + \tau_{xz}) \quad (8)$$

The axial stress state has the distortion energy with respect to the failure. The energy can be expressed by using the equation

$$U_{oD} = \frac{1}{12G}(\delta_{ekv}^2 + \delta_{ekv}^2) \quad (9)$$

When equations 8 and 9 are marked as equal, the reference stress σ_{ekv} can be solved from the expression

$$\sigma_{ekv} = \sqrt{\delta_x^2 + \delta_y^2 + \delta_z^2 - \delta_x\delta_y - \delta_y\delta_z - \delta_x\delta_z + 3(\tau_{xy}^2 + \tau_{yz}^2 + \tau_{xz}^2)} \quad (10)$$

The expression is qualified in the main coordinate system and it can be transformed into the expression

$$\sigma_{ekv} = \sqrt{\sigma_1^2 + \sigma_2^2 + \sigma_3^2 - \sigma_1\sigma_2 - \sigma_2\sigma_3 - \sigma_1\sigma_3} \quad (11)$$

As a result, the hypothesis gives the reference stress for the yield strength. This stress is also called the von Mises stress. The reference stress can be used in the rainflow simulation for the determination of the fatigue life. (Outinen 2007, 349-350)

The fatigue life calculations usually require known loading history. Most of the fatigue analyses are adaptable for the loading which has constant amplitude. In this case, the spring was under the random cyclic loading. Figure 22 shows the process of the universal fatigue analysis in the time domain. The process can be applied to any kind of random loading fatigue analyses in time domains. (Aruduru 2004, 24)

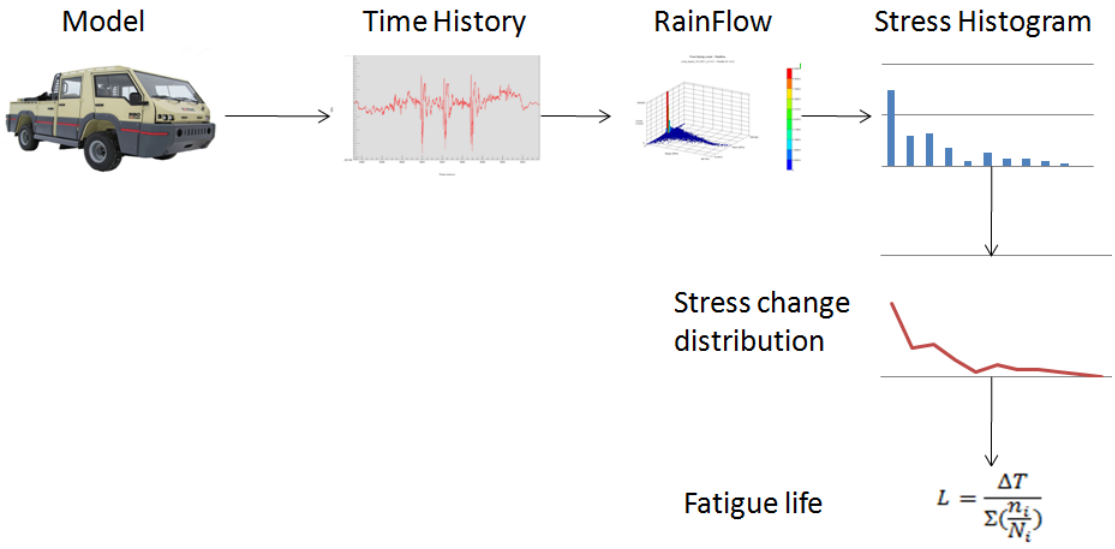

Figure 22. The universal process of the fatigue analysis in variable amplitude loading. (Aruduru 2004, 25)

An example of the random stress history is presented in Figure 23. The determination of the stress or loading history requires information from measurements. Measure-

ments can be processed by using varying methods. In this case, measurements were done by using strain gages.

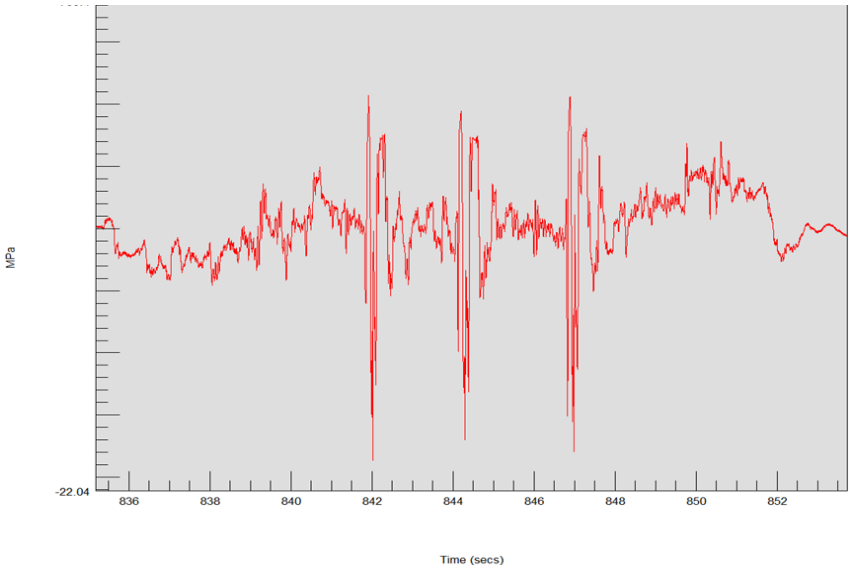

Figure 23. Variable amplitude stress history.

The rainflow is a counting algorithm which was developed by M. Matsuiski and T. Endo. Principles of the algorithm are based on the behaviour of the material with respect to the stress and strain. The algorithm calculates the highest stress changes occurred in the test. After the determination of the rainflow count, the stress is converted to a histogram. The histogram points out the number of loading count in stress levels. (Aruduru 2004, 24-25)

After the determination of the cycle count, each cycle must be classify by using the S-N curve. Each stress level corresponds to a load change number in the S-N curve with respect to the fatigue strength. The Miner's cumulative damage theory is capable to process the fatigue under the variable loading. The theory was presented and developed by A. Palmgren and M.A. Miner. The principle of the theory is that the certain amplitude in the stress state consumes the proportional part of the structure life time. The life time assessment can be calculated from the equation

$$L = \frac{\Delta T}{\Sigma(\frac{n_i}{N_i})} \tag{11}$$

where ΔT is the time taken to a test, n_i is the load count from the rainflow and N_i is the load count from the S-N curve. The sum of n_i/N_i is the portion of the life time which is elapsed in the test. (Outinen 2007, 395)

The life time in variable amplitude loading can be also evaluated with the strain life based approach with the Morrow's mean stress correction. The Morrow's strain life model can be expressed with the equation

$$\varepsilon = \frac{\sigma'_f}{E}\left(1 - \frac{\sigma_m}{\sigma'_f}\right)(2N_f)^b + \varepsilon'_f(2N_f)^c \quad (12)$$

Where ε is a strain amplitude, E is a modulus of elasticity, N_f is a number of reversals to failure, σ'_f is a fatigue strength coefficient, b is fatigue strength exponent, ε'_f is a fatigue ductility coefficient and c is a fatigue ductility exponent. These material values are introduced in chapter 3.9. (Abdullah, S. Ahmand, F.N. Jalar, A. & Chua, L.B 2009, 352)

3.9 Material Properties

The material of the spring steel was, according to the spring's manufacturer, SUP 9 (JIS). Standard comparison indicated that the SUP 9 spring steel is equal to the 55Cr3 spring steel in European standards. Society of Automotive Engineers (SAE) number for the 55Cr3 is 5160. Fatigue properties of the steel were determined according to SAE from the GlyphWorks material properties database. Material values from the finish standards association's standard SFS-EN 10089 and from the Glyphworks material database are presented in Table 1. The standard comparasion chart can be viewed from Appendix 8.

Table 1. Material properties (GlyphWorks, Material database)

Material Properties		
SAE5160/SUP 9/55Cr3		
Elastic Modulus, *E*	207	GPa
Yield Strength, R_{eL}	1250	MPa
Ultimate tensile strength, R_m	1600	MPa
Work Hardening Coefficient, *K*	1940	MPa
Fatigue Strength Coefficient, $S_{f'}$	2063	MPa
Cyclic Strength Coefficient *K'*	2432	MPa
Work Hardening Exponent, *n*	0.05	
Fatigue Strenght Exponent, *b*	-0.08	
Fatigue Ductility Exponent, *c*	-1.05	
Fatigue Ductility Coefficient $E_{f'}$	9.56	
Cyclic Strain-hardening Exponent, *n'*	0.13	
Cut-off, N_c	2.00E+08	Reversals

The accurate information of the fatigue properties was not available for this study. Usually the availability of S-N curves is not good and this sets limits to the design with respect to the fatigue. However, the estimation of the S-N curve was determined according to Airila (1997, 22). The S-N curve is shown in Figure 24.

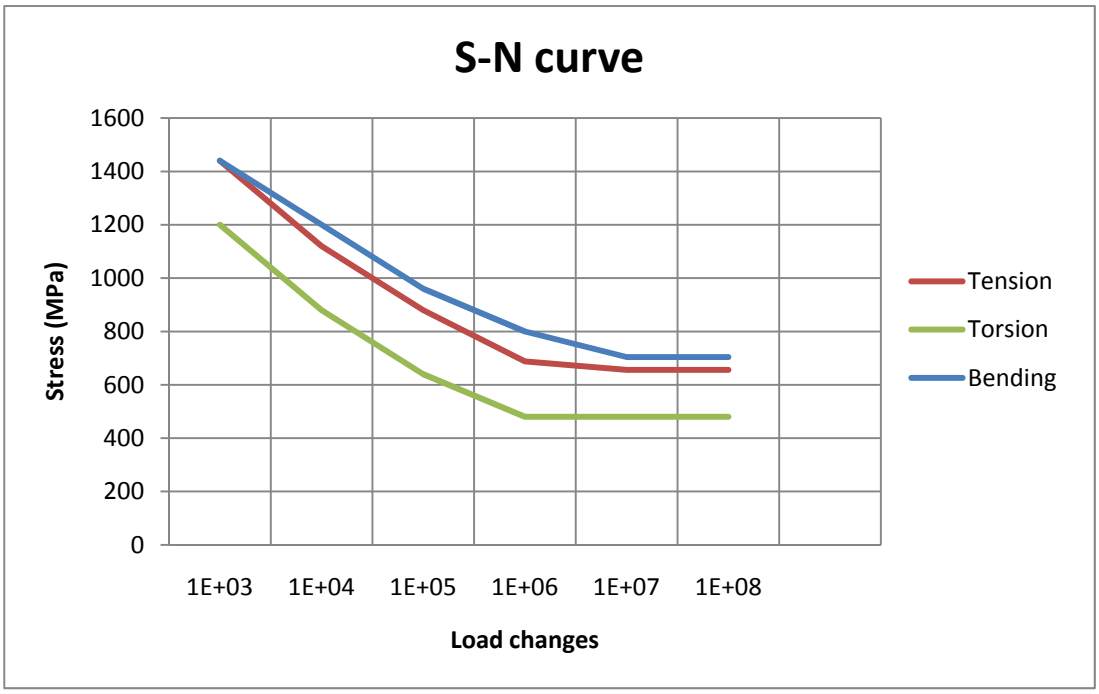

Figure 24. Rough estimation of the S-N curve for the 55Cr3 spring steel. (Airila, 1997, 22)

4 MEASUREMENTS

4.1 Instruments and Installation

Measurements were carried out by using strain gages. The gage type was rectangular triaxial stacked rosette manufactured by Kyowa. The gage type according to the manufacturer was KFG-5-12D17-11L1M2S. The properties of the gage are shown in Table 2. Strain gages were installed in one front spring and one rear spring to fixed support side.

Table 2. Gage properties

KFG-5-120-D17-11L1M2S		
Gage factor	2.12	
Transverse sensitive	0.4	%
Resistance	120 ± 0.4	Ω
Operating temperature	-196 to 120	˚C
Temperature compensation	±1	µm/m/˚C

The surface had to be polished because it contained paint and scales from the manufacturing process. Installations were done by using an adhesive mounting method. Locations of gages were determined by using the FE analysis as an input data. The analysis gave a suggestive examination point for stress measurements. Installations are shown in Figure 25.

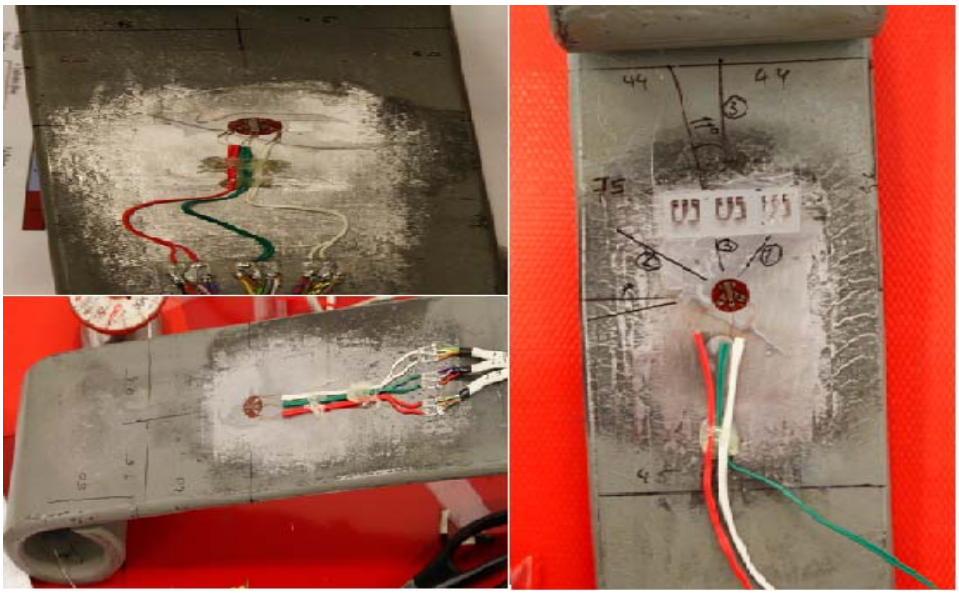

Figure 25. Installation of strain gages

4.2 Calibration

Calibration was done by using output data from the FEM. Analysis was carried out by loading the single leaf. Loading for calibration was 208 N. The calibration model's boundary conditions and loading is presented in Figure 26.

Microstrains from the calibration and from the FEA are shown in Table 3. The signal did not suffer any drastic interference. The calibration results indicated that strain gages are working properly and no filtering in the signal processing is needed to carry out actual measurements. The calibration results can be viewed from Appendix 6.

Table 3. Calibration results.

ANSYS		STRAIN GAGES	
Microstrains		Microstrains	
εx	62.51	εx	76.24
εy	-20.36	εy	-18.74
εz	-12.24	εz	-18.50

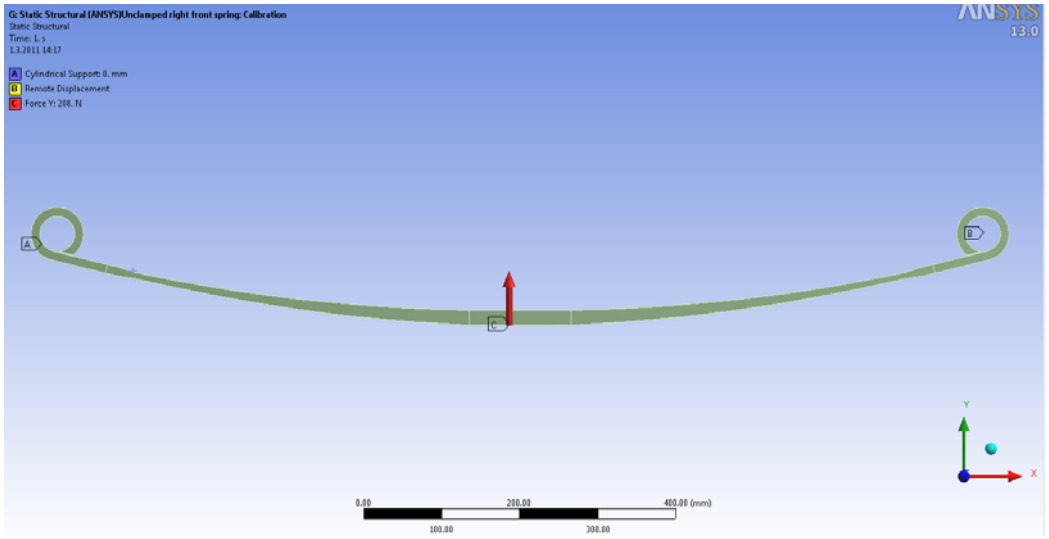

Figure 26. Support and loading for calibration.

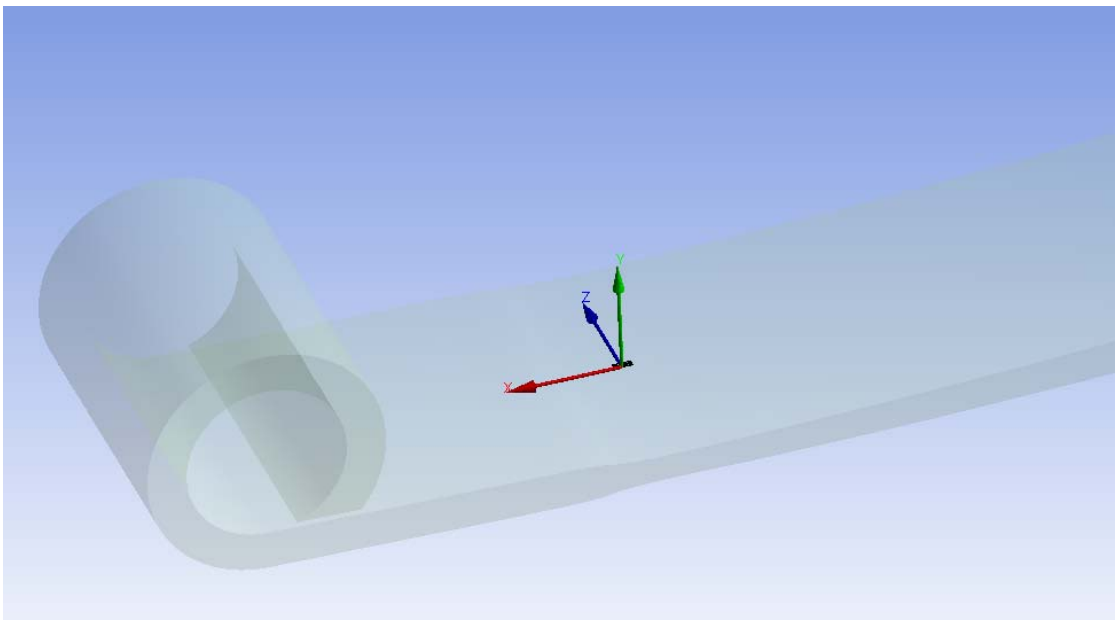

Figure 27. Location of the upper strain gage rosette.

4.3 Environments

Measurements were done in the Normet test drive track. The test was divided to three different runs. The run one was done by driving in the smooth road. Run included normal actions like turning, braking and accelerating. Run two simulated direct impact to the right front wheel. Run three was created to the environment which corresponded impact situation in the curve driving to the right front wheel. The test settings for measurements can be viewed in Appendix 5.

4.4 Post-Processing of the Data

The data from measurements was processed by using the Glyphworks program which is designed for the processing of large amount of data. The program is capable to process the recorded time domain data from measurements. In this case the data was imported to the program as a strain data. The calculation process is shown in Appendix 9. Recorded data was converted to the Von-Mises stress, maximum principal stress and maximum principal strain by using the rosette tool. The rosette tool calculates the wanted variable directly from three channels which represent the single rosette. The strain life based fatigue calculations were done in the Glyphworks. Determinations of the rosette tool settings were based on the material and strain gage properties. The calculated stress was processed to loading cycles with the rainflow algorithm.

5 RESULTS

5.1 Dynamic Simulation

The dynamic simulator was used in to measure forces and moments. Forces and moments were calculated from a constrain point between the spring and the axle. The constrain point is shown in Figure 29, where the x axis is red, the y axis is green and the z axis is blue. The simulation environments were created to correspond to measurement environments. Precise synchronisation was not possible because the test track conditions were variable due to weather conditions. The simulation was processed in normal driving and impact situations. Normal driving loads were determined from the situation which corresponds to driving in an asphalt road. Impact loading was determined from the pothole impact. The transitional velocity at impact moment was 9.5 m/s. Maximum values from dynamic simulation can be viewed from Table 4. F_x is a longitudinal loading, F_y is a vertical loading and F_z is a lateral loading. The moment T_x is over the x axis Results were used as an input values to the FEA to determine theoretical stress levels of the spring.

Maximum values in normal driving are produced from braking situations. These can be considerate as normal events when vehicle is driven in a mine. Roads in a mine environment are mostly built to a spiral shape. This means that the vehicle is under constant curve drive.

Results from the dynamic simulation are not available on public report.

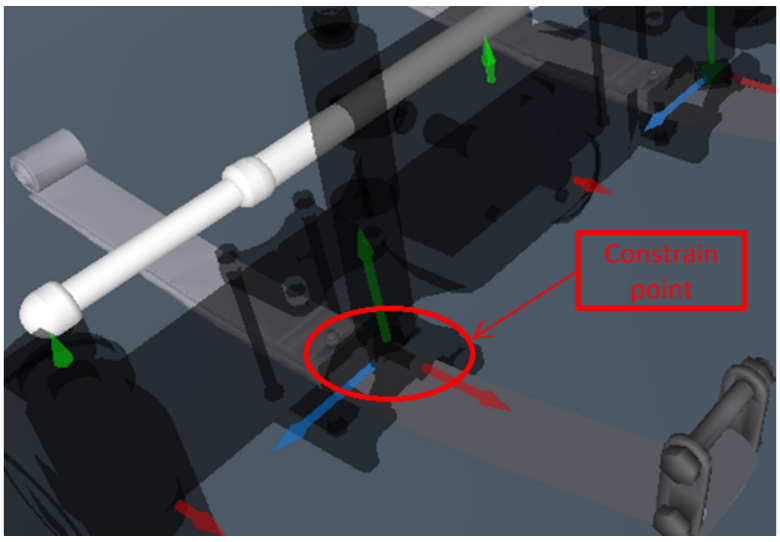

Figure 29. The constrain point of the spring and axle.

5.2 FEM

5.2.1 Static Loading

The first step of the FEA was to calculate the spring under the static loading. This loading case indicated that the stress is distributed equally in the static loading. The static load was determined from the axle mass of the vehicle. The distribution of the axle mass for the single spring in the front axle was 14700 N. Stress distribution is shown in Figure 30. The displacement of the spring is shown in Figure 31. In theoretic loading situation the spring is almost straight.

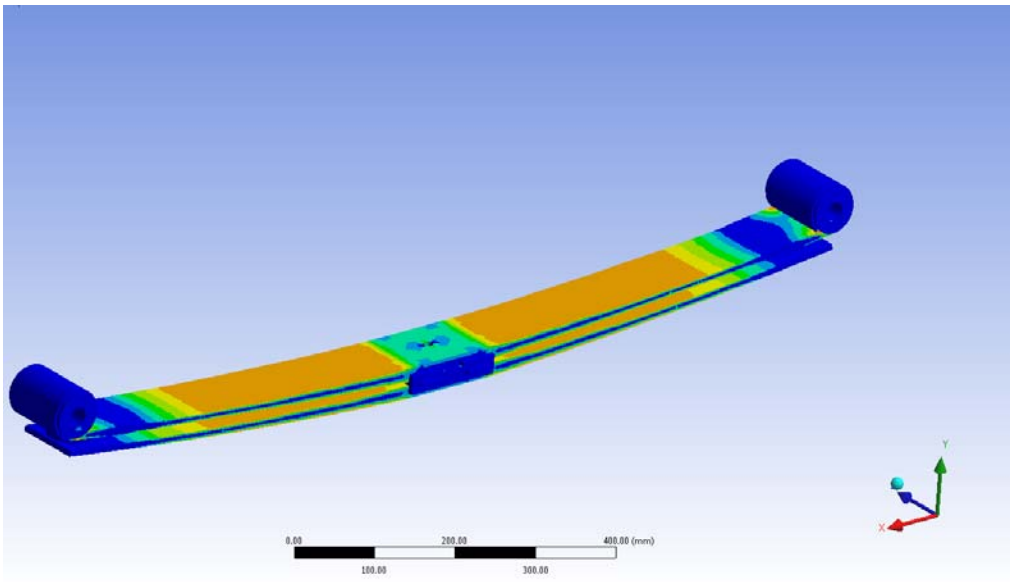

Figure 30. Von-Mises stress distribution in static loading.

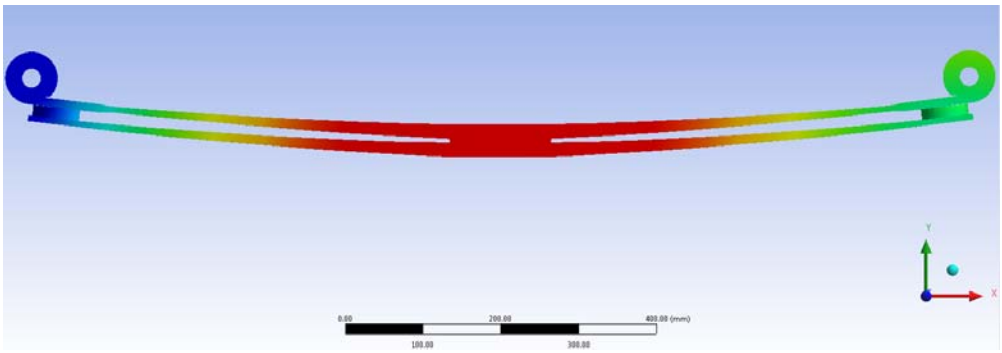

Figure 31. Displacement in static loading.

5.2.2 Normal Driving Loads

Normal driving loads were determined from the dynamic simulator. Input forces are maximum values from braking situations in the mine environment. Figure 32 shows the stress concentration area which is generated in the thinnest point of the spring.

The deformation shape of the spring is presented in Figure 33. The shape of the spring is twisted to a small S curve. This is due to torque caused by axle's movement in lateral direction.

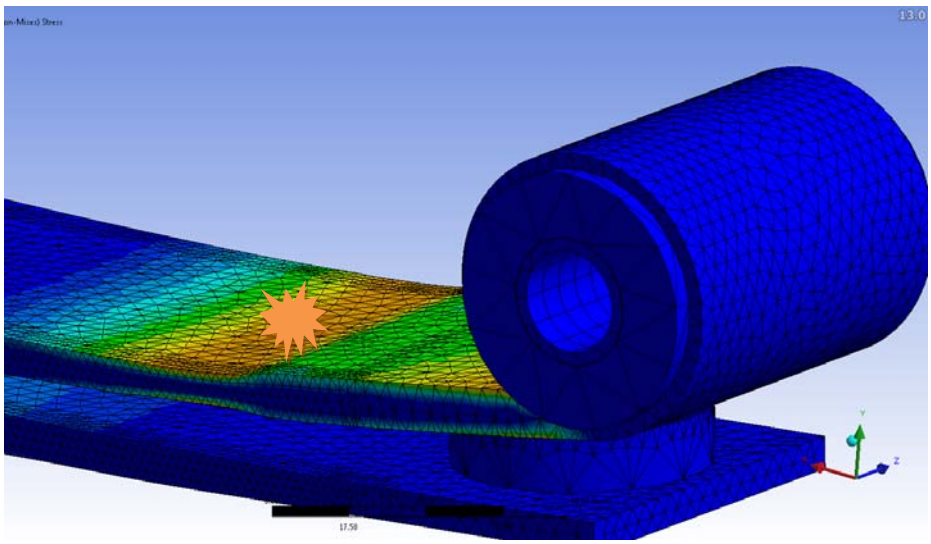

Figure 32. Von Mises stress in examination point.

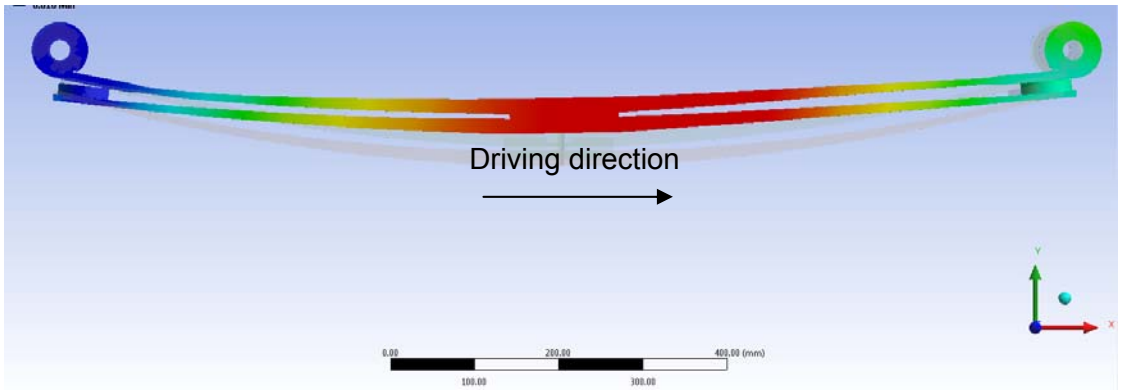

Figure 33. Total deformation in normal driving.

5.2.3 Impact Loads

Input loading for the impact simulation was determined from the dynamic simulator. Maximum von Mises stress is not available in public report. Examination point was located in thinnest point of the spring in the fixed support side.

The total deformation of the spring in impact is shown in Figure 35. Figure indicates that spring is twist to a large S curve. The S curve causes high stress concentration to the fixed support side. The analysis did not show any deformation in the z axis.

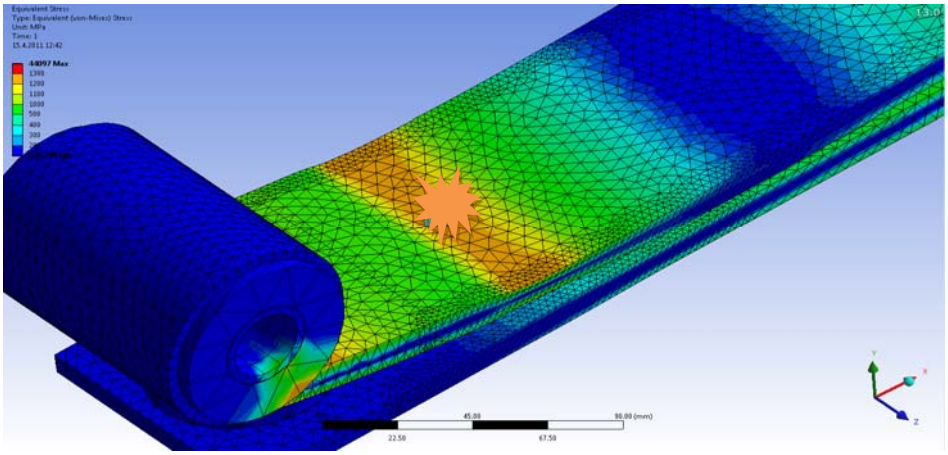

Figure 34. Von Mises stress in the fixed support side.

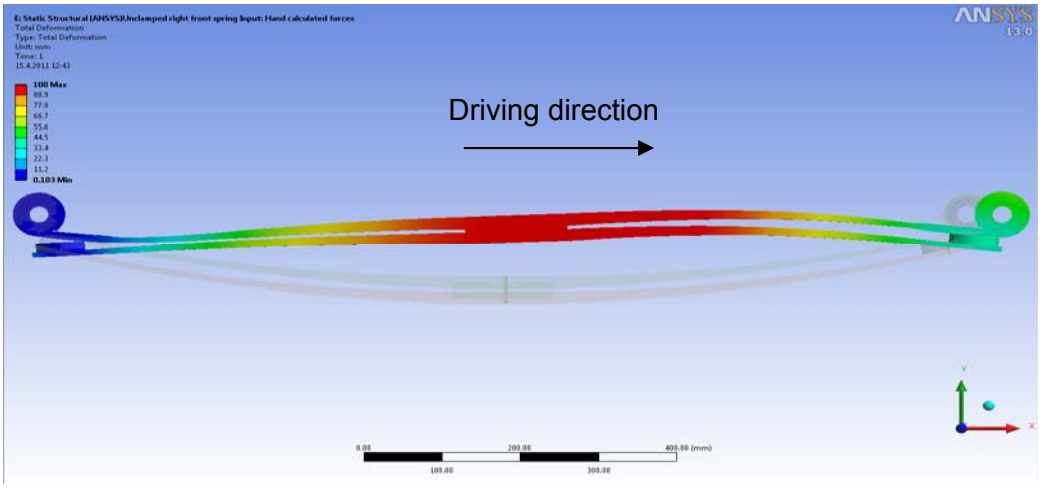

Figure 35. Deformation of the spring in impact.

5.3 Measurements

The purpose of measurements was to determine the actual stress levels of the spring in different conditions. Each run contained different amount of peak values. Figure36 shows von Mises stresses from the clamped and unclamped front spring. Results were recorded from curve drive. Figure indicates that results from the clamped and unclamped spring are almost equal.

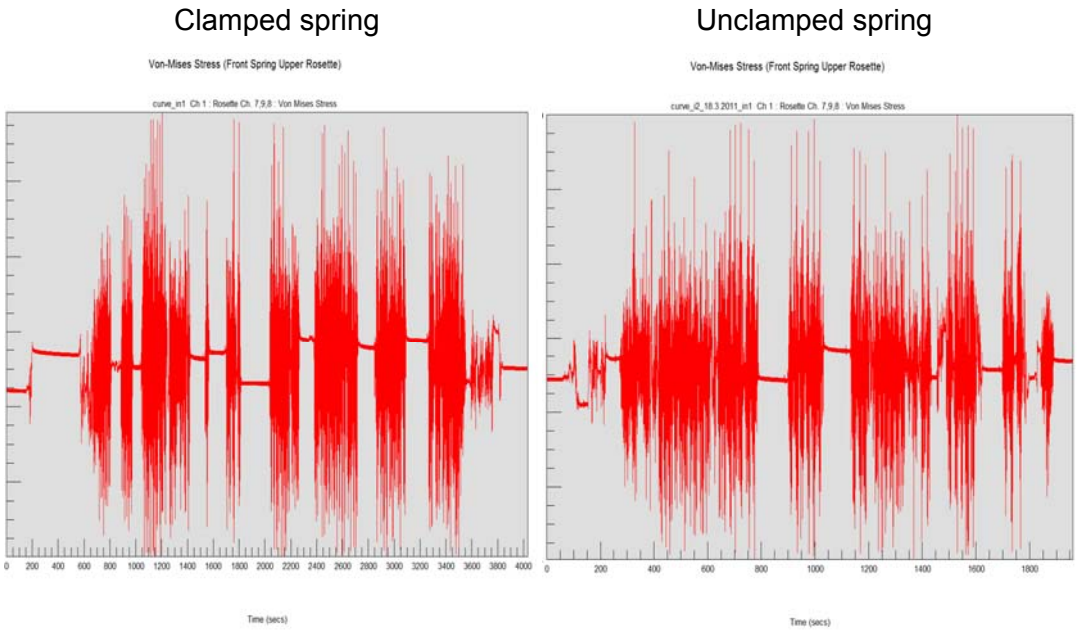

Figure 36. Von Mises stresses from measurements

6 ANALYSIS OF THE RESULTS

The main object of the project was to determine the effect of improvement in spring's structure. The force in the direction of the z-axis did not produce any displacement to the spring in the FEA. Magnitude of the force was quite small in the dynamic simulation. FEA did not shown any difference between the unclamped and clamped spring because the stress was created from forces in y and x axis. Magnitude of the torque moment over the x-axis was also quite small in the dynamic simulation. The comparison chart of the theoretical and experimental stress levels is shown in Table 4. Results for the examination were defined from the static loading, normal driving and from curve driving. Deviation between theoretical and experimental result in normal driving stress was 21 % and in curve drive 5 %. Errors between results are products from simplifications done in FEA and from difference between simulation and measurement environments. The deviation in static stress values is quite high. Explanation for this is that the spring's initial position is different than in the FEA. In the FEA, the deformation of the spring is similar to ideal case. Figure 37 shows the deformation of the spring under the vehicle. Figure indicates that the spring is twisted to the curve in static loading and it creates high static stress to the examination point. The deviation between results can be considerate acceptable.

Figure 37. The deformation of the spring.

Table 4. Deviation of results

Deviation between Ansys and measurements	
	Deviation
Static Stress	66 %
Normal Driving Stress in Breaking	21 %
Curve Driving Stress	5 %

The analysis indicated that stress in the thinnest point of the front spring was too high. Also the auxiliary leaf does not support the main leaf. This causes that lateral loading is directed to the main leaf and the auxiliary leaf takes only vertical loading. When breaking and accelerating, the spring is twisted to a S curve. The profile can be considered acceptable for normal driving but not for the harsh mine environments where suspension is under heavy impacts.

The fatigue analysis was carried out by using the von Mises stress, maximum principal stress and maximum principal strain. Evaluations were done with respect to bending. The idea was to compare results from different kind of methods. The maximum principal stress gave the shortest life time. The von Mises stress and the maximum principal strain gave approximately the same life time for the spring. Differences between fatigue analyses were that the strain life based approach used more accurate material information. The stress life based calculations were done from the S-N curve. The curve was determined with rough estimation because the accurate information was not available.

According several customers reports, the life time of springs were changing from 100 engine hours to few months. The results from measurements are not directly comparable to customer's reports because the amount of load changes is determinative in the fatigue analysis.

Results are indicating that the main reason for the spring failure is pre-mature fatigue fracture. The fracture will occur after the relatively short period of time because the stress levels of the spring are high in the rough environment. The reason for high stress levels in the fixed support side are longitudinal forces which are forcing the spring to the S curve.

7 SUMMARY OF THE PROJECT

7.1 Results

The purpose of the final project was to analyse the leaf spring failure in a mining machine. The research was concentrated on defining the stress levels from the most common fracture location. Definitions of stress levels in springs were done with theoretical and experimental methods. The theoretical phase consisted of dynamic simulations, finite element and fatigue analyses. The experimental phase consisted of strain gage measurements. Stress levels magnitudes from measurements were verified by using finite element analysis.

As a result, the effect of improvements was determined and the reason for the actual failure was solved. The results also acted as a criterion for the new design of the spring for the RBO. Springs were designed in cooperation with the spring manufacturer.

Accurate results are not presented in the public version of this report by request of the customer. This final project has been evaluated and accepted as a whole.

7.2 Further Development Subjects

The project did not include a wider analysis and testing of the new spring. From the theoretical point of view, the solution should give longer life time for springs. The analysis of the new spring can be carried out by using this report as a guideline. The RBO has problematic solution in the axle construction, which affects the life time of the suspension components. If the new solution does not provide the wanted life time to springs, supporting of the axle to the body should be considered.

7.3 Conclusions

Overall the project was successful because the reason for the failure was solved in the general outline. The project also produced the design of new springs to the RBO. The original project plan included the force and acceleration sensor measurements which had to be left outside the project. This was due to problematic measurement

conditions which prevented the proper installation of force sensors to the spring structure. Allocated resources were also a problem for acquiring instruments. The pre-analysis with the FEM indicated that strain gage measurements could give effective information about the cause of the fracture. The project did not include fracture mechanics approach, because there were no broken springs available. Fracture mechanics could have also verified results from measurements and calculations. The definition of the project was carried out successfully even though it changed a little during the project. Changes had no remarkable effect on the schedule. The work load stayed reasonable.

The subject of the project was quite interesting. It included new theories which were not familiar from earlier studies. This was also quite motivating because of the change to learn new and essential theories in machine design. The subject turned out to be more complex than expected. The definitions and synchronisation of theoretical and experimental conditions were probably the most challenging task. Assumptions and precise determination of the physical problem at the beginning of the project helped to stay in the right direction during the project.

The educational purpose of the project was remarkable for the learning process. It taught how to apply known theories to a unique problem. The project also confirmed more and more the importance of the proper project plan and preparations. Synchronisation of the dynamic simulation and measurements demanded systematic work and evaluation of different variables. The analysis required familiarising with simulation programs such as the MeVEA’s dynamic simulator, the Ansys Workbench 13.0 and the GlyphWorks.

REFENCES

Abdullah, S. Ahmand, F.N. Jalar, A. & Chua, L.B. P2009, Life Assessment of a Parabolic Spring Under Cyclic Strain Loading. European Journal of Scientific Research, Eurojournal Publishing. Available on: http://www.sciencedirect.com/

Airila, M. Ekman, K. Hautala, P. Kivioja, S. Kleimola, M. Martikka, H. Miettinen, J. Niemi, E. Ranta, A. Rinkinen, J. Salonen, P. Verho, A. Vilenius, M. & Välimaa, V P.1997, Koneenosien suunnittelu. Helsinki: Werner Söderström Osakeyhtiö.

Aruduru, S. P. 2004. Fatigue life calculation by rainflow cycle counting method, Middle East Technical University.

Farmi Forest, Company presentation, read 22.3.2011. Available on:www.farmiforest.fi

GlyphWorks, Material Database

Hoffmann, K. P.1989. An Introduction to Measurements Using Strain Gages. Darmstad: Hottier Baldwin Messtechinik GmbH.

Laine, O. P.1981. Autotekniikka 2. Tampere: Sonator.

Korkealaakso, P. P.2009. Real-time simulation of mobile and industrial machines using the multibody approach. Lappeenranta: Lappeenranta University of Technology.

Kulmala, J. 2005. Rugged design goes underground. MachineDesign.com. Read 19.2.2011. Available on: www. machinedesign.com

MacDonald, B P.2007. Practical Stress Analysis with Finite Elements. Ireland: Glasnevi Publishing.

MeVEA Oy, Manual, Normet RBO Simulation Model, 2010. Not available publicly

MeVEA Oy, Manual, Reference Manual for Solver Libarary. Not available publicly

Nakhaie Jazar, G. P.2008 Vehicle dynamics: Theory and applications. USA: Springer. Available on: http://books.google.com

Normet Group, Press release, read 22.3.2011. Available on: www.kauppalehti.fi

Normet Group, RBO product description, read 22.3.2011. Available on:www.normet.fi

Normet Company Presentation, 2011. Not available publicly

Zahavi, E. & Barlam, D. P.2001. Nonlinear Problems in machine design. CRC Press.

Outinen, H. Salmi, T. & Vulli, P. P. 2007. Lujuusopinperusteet. Tampere: Klin-gendahl Paino Oy.

Rouvinen, A. P.2003 Mekasnimien dynamiikan simuloinnissa sovellettavia numeerisia- ja mallinnusmenetelmiä. Lappeenranta: Lappeenrannan teknillinen yliopisto, Konetekniikan osasto.

SFS-EN 10089 2003. Hot-rolled steels for quenched and tempered springs. Technical delivery conditions. 2007. Helsinki. Finnish standards association SFS.

SFS-EN ISO 26909 2010. Springs. Vocabulary. 2010 Helsinki. Finnish standards association SFS.

Stress-strain-diagram, Read 15.3.2011. Available on: http://www.mathalino.com

Vishay Micro-Measurement. The three-wire quarter bridge circuit, Application note TT-612, 2005 Read 8.4.2011. Available on: www.intertechnology.com

www.savonia.fi